



ORIGINAL PAPER

Pembe Merve Karabulut · İlkem Turhan Çetinkaya ·
Hüseyin Oğuz · İsa Çömez

Moving contact problem of a functionally graded orthotropic coated half plane

Received: 7 December 2023 / Revised: 5 February 2024 / Accepted: 10 March 2024
© The Author(s) 2024

Abstract This paper develops a frictional moving contact model for a functionally graded (FG) orthotropic layer pressed by a rigid cylindrical punch. The FG orthotropic layer is fully bonded to the isotropic half-plane. The punch moves to the left on the layer at a constant subsonic velocity and a shear stress arises in the contact zone according to the Coulomb friction law. General expressions of displacements and stresses are derived with the help of the Fourier transform and Galilean transformation. Using boundary conditions, the moving contact problem is reduced to a Cauchy-type singular integral equation, the unknowns of which are contact stress and contact width. Gauss–Jacobi integration formula is used to solve the obtained singular integral equation. The effect of some parameters and material properties on the contact width, contact stress and in-plane stress are given in graphical forms and detailed numerical interpretations are presented.

1 Introduction

Contact problems play an important role in mechanics because of their wide application to many engineering problems, such as foundations, pavements in roads and runways, railway ballast, brake disks, and gas turbines. Due to their advanced mechanical properties, functionally graded materials (FGMs) have been widely used in various engineering practices. The usage of FGMs as a coating layer or an interfacial material reduces mismatching stresses, increases the bonding strength, improves surface properties, and provides protection against adverse thermal or chemical environments [1, 2]. Some of the applications of FGMs are cylinder linings, brake disks and other automotive components for the purpose of improving the wear resistance of abrasion seal design in stationary gas turbines [3]. Numerous studies on FGMs have been conducted recently. For example, Draiche et al. [4] developed an integral shear and normal deformation theory for functionally graded (FG) sandwich curved beams. Free vibration analysis of FG sandwich beams, and two-dimensional FG structures with an exponential material gradation were presented by Yang, Lam et al. and Yang, Kou et al. respectively [5, 6]. A formulation for analyzing FG sandwich structures was presented by Rezaiee-Pajand et al. [7] who developed a mixed interpolated formulation for nonlinear analysis of plates and shells. Xu and Meng [8] presented beam models for FGMs with regular polygonal cross sections, while Chikh [9] presented an analytical solution to a problem of isotropic homogeneous beams based on an elastic foundation.

Among the contact problems, the moving punch problem has a separate and important place. Since, if the speed of the rigid body relative to the elastic one is small enough, then the dynamic character of the

P. M. Karabulut (✉)
Department of Civil Engineering, Engineering Faculty, Cankırı Karatekin University, Çankırı, Turkey
e-mail: pembemervekarabulut@karatekin.edu.tr

Ilkem T. Çetinkaya · H. Oğuz
Department of Mathematics, Science and Art Faculty, Kütahya Dumlupınar University, Kutahya, Turkey

İsa Çömez
Department of Civil Engineering, Engineering Faculty, Karadeniz Technical University, Trabzon, Turkey

phenomenon could be neglected. However, there are problems that arise in practice in which the speed of one body relative to the other is quite large, and, therefore, we need to investigate whether it is necessary to take the dynamic character of the problem into account [10]. Some studies on the moving contact problem are as follows:

Balcı and Dag [11–14] reduced moving contact problems to singular integral equations and presented a detailed mechanical analysis. Chen and Chen [2] considered a thermoelastic contact model sliding at a speed V on a finite graded layer in which the determination of stress intensity factors (SIFs) and contact stresses were given. A frictional moving punch problem for orthotropic materials was presented for different punch cases by Zhou et al. [15], the study leading to the explanation of the surface damage mechanism of orthotropic materials. The exact solution of moving triangular or parabolic punch problems was presented by Zhou et al. [16]. Meanwhile, Zhou and Lee [17] presented an eigenvalues analysis for a moving frictional punch problem and Çömez [18, 19] considered frictionless and frictional moving contact problems, respectively. The obtained singular integral equations were solved by Gauss–Chebyshev and Gauss–Jacobi integration formulas, respectively. Güler [20] considered a frictional moving contact problem in which a rigid cylindrical punch was assumed to slide at a constant velocity on an orthotropic layer attached to an isotropic half-plane. A singular integral equation was obtained with the help of the Fourier transform technique and Galilean transformation. Numerical results were obtained with the help of the Gauss–Jacobi method. Çömez [21] also applied the singular integral equation technique to a sliding moving contact problem in which the FG layer was bonded to an isotropic homogeneous layer. Zhou and Kim [22] employed the Galilean transformation and Fourier transforms to a frictional moving contact problem of piezomagnetic materials to obtain Cauchy integral equations. Numerical analysis revealed the effects of the friction coefficient and the moving speed of the punch.

In the application of contact mechanics, material properties have great importance. The materials can be classified as isotropic and anisotropic. While isotropic materials have the same properties in all directions, anisotropic materials have different properties in different directions. In particular, the mechanics of anisotropy are of interest when increasing the usage of anisotropic materials such as composites. Among the anisotropic materials, orthotropic materials, in which their mechanical and thermal properties are unique and independent in three mutually perpendicular directions, have been used in many applications, such as fiber-reinforced plates and shells, thin films, and coatings. Bagheri et al. [23] and Bagheri and Hosseini [24] considered multiple moving crack problems in a non-homogeneous orthotropic strip and a non-homogeneous orthotropic plane, respectively. Numerical results were presented for material properties. Hashemi and Ayatollahi [25] examined the transient behavior of an orthotropic layer in multiple crack problems while another multiple crack problem in an orthotropic non-homogeneous plane was studied by Mottale et al. in [26]. Lobatto-Chebyshev method was applied to present the material orthotropy on SIFs. Lei et al. [27] applied the generalized finite difference method to crack problems for anisotropic materials, the numerical results given for orthotropic materials. Yusufoglu and Turhan [28, 29] solved an orthotropic strip problem using different methods for thick and thin strips, respectively Erbaş et al. [30] considered an orthotropic strip problem and solved it with an iterative solution technique and a direct asymptotic procedure for thick and thin strip cases, respectively. Rodriguez-Tembleque and Abascal [31] presented a new methodology for 3D frictional contact problems, while Pozharskii [32] approached a 3D contact problem in orthotropic half-space numerically and analytically. An orthotropic plane problem with a slit was considered by Hakobyan and Dashtoyan [33] and an exact solution presented. Shavlakadze et al. [34] used the methods of the theory of analytic function to reduce the contact problem for a piecewise homogeneous orthotropic plate to a system of singular integro-differential equations, Hou et al. [35] proposed a method based on the Green's function for the orthotropic coating-substrate system and Ustinov and Idrisov [36] calculated two modes of SIFs for the problem of two strips of different degenerate and non-degenerate orthotropic materials. Finally, Cao et al. [37] examined the effect of the material orthotropy in a frictional receding contact problem.

Although there are many studies in the literature where the punch is static, the number of studies involving the moving contact problem is relatively very few. On the other hand, moving contact studies involving FG half-planes and layers are fewer than homogeneous studies. More specifically, there are no studies on the moving contact problems of an FG orthotropic layer bonded to a homogeneous isotropic half-plane. To fill this gap in the literature, the moving punch problem is modeled with the help of elasticity theory and boundary conditions of the problem in the view of the basics of elasticity theory. This study consists of six sections. The second section defines the boundary conditions and formulation of the problem. In the third section, the singular integral equation is derived, the fourth section is devoted to the numerical solution of singular integral

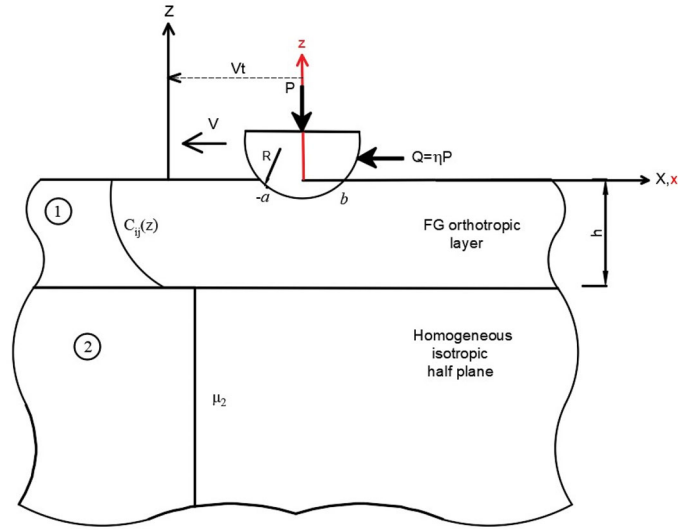


Fig. 1 Geometry of frictional moving contact problem

equations and the fifth section is devoted to the numerical results and mechanical interpretation. Finally, the last section is the conclusion.

2 Problem statement and formulation

This section presents the formulation of a frictional moving contact problem of an FG orthotropic layer bonded to a homogeneous isotropic half-plane (see Fig. 1). It is assumed that the thickness of the FG orthotropic layer is h and the punch profile is cylindrical. The rigid punch with a radius R moves frictionally at a constant velocity V in the negative direction of the $-x$ axis. The rectangular coordinates (X, Z) are fixed in the layer and the translating coordinates (x, z) are attached to the moving punch. It is modeled that the punch and layer are in relative motion, that is, $Q = \eta P$. Where η is the coefficient of friction, P and Q are the resultant normal and tangential forces, respectively.

The boundary conditions of the problem can be defined as:

$$\sigma_{z1}(x, 0) = \begin{cases} -p(x) & -a < x < -b \\ 0 & x \leq a, x \geq b \end{cases} \quad (1a)$$

$$\tau_{xz1}(x, 0) = \begin{cases} -\eta p(x) & -a < x < -b \\ 0 & x \leq a, x \geq b \end{cases} \quad (1b)$$

$$u_1(x, -h) = u_2(x, -h) \quad (1c)$$

$$w_1(x, -h) = w_2(x, -h) \quad (1d)$$

$$\sigma_{z1}(x, -h) = \sigma_{z2}(x, -h) \quad (1e)$$

$$\tau_{xz1}(x, -h) = \tau_{xz2}(x, -h) \quad (1f)$$

where σ_{zi} ($i = 1, 2$) and τ_{xzi} ($i = 1, 2$) are stress components; u_i ($i = 1, 2$) and w_i ($i = 1, 2$) are displacement components, $p(x)$ and η are the contact stress under the rigid punch on the contact area $(-a, b)$ and the friction coefficient, respectively.

Now, we will give some basic equations of elasticity theory. Motion equations without body forces can be written as

$$\frac{\partial \sigma_{xi}}{\partial X} + \frac{\partial \tau_{xzi}}{\partial Z} = \rho_i(z) \frac{\partial^2 u_i}{\partial t^2} \quad (2a)$$

$$\frac{\partial \tau_{xzi}}{\partial X} + \frac{\partial \sigma_{zi}}{\partial Z} = \rho_i(z) \frac{\partial^2 w_i}{\partial t^2} \quad (2b)$$

where σ_{xi}, u_i, w_i, t and ρ denote the X – components of the stress, X – and Z – components of the displacement vector, time variable and density, respectively.

The generalized Hooke's law for an FG orthotropic material in a state of plane strain can be written as follows.

$$\sigma_{x1} = C_{11}(z)\frac{\partial u_1}{\partial X} + C_{13}(z)\frac{\partial w_1}{\partial Z} \quad (3a)$$

$$\sigma_{z1} = C_{13}(z)\frac{\partial u_1}{\partial X} + C_{33}(z)\frac{\partial w_1}{\partial Z} \quad (3b)$$

$$\tau_{xz1} = C_{55}(z)\left(\frac{\partial u_1}{\partial Z} + \frac{\partial w_1}{\partial X}\right) \quad (3c)$$

where $C_{ij}(z)$ are the elastic stiffness constants and their continuous variation is modeled by an exponential function in the following form:

$$C_{ij}(z) = C_{ij}^0 e^{\gamma z}, \quad \gamma h = -\text{Log } \Gamma, \quad \Gamma = C_{ij}^h / C_{ij}^0 \quad (4)$$

where γ and Γ denote the inhomogeneity constant and the ratio of material constants on the top and bottom surfaces of the FG orthotropic layer, respectively. It is assumed that the variation of the Poisson's ratio is constant.

The following Galilean transformation is suitable to use for the constant speed:

$$x = X - Vt, \quad z = Z \quad (5)$$

Substitution of the generalized Hooke's laws (3) and Galilean transformation (5) into motion Eq. (2) yields the steady-state governing equations in the coordinate system (x, z) .

$$C_{11}^0 \frac{\partial^2 u_1}{\partial x^2} + C_{55}^0 \frac{\partial^2 u_1}{\partial z^2} + (C_{13}^0 + C_{55}^0) \frac{\partial^2 w_1}{\partial x \partial z} + \gamma C_{55}^0 \left(\frac{\partial u_1}{\partial z} + \frac{\partial w_1}{\partial x} \right) = c_1^2 C_{55}^0 \frac{\partial^2 u_1}{\partial x^2} \quad (6a)$$

$$(C_{13}^0 + C_{55}^0) \frac{\partial^2 u_1}{\partial x \partial z} + C_{55}^0 \frac{\partial^2 w_1}{\partial x^2} + C_{33}^0 \frac{\partial^2 w_1}{\partial z^2} + \gamma \left(C_{33}^0 \frac{\partial w_1}{\partial z} + C_{13}^0 \frac{\partial u_1}{\partial x} \right) = c_1^2 C_{55}^0 \frac{\partial^2 w_1}{\partial x^2} \quad (6b)$$

where $c_1^2 = V^* = V^2 / (C_{55}^0 / \rho_{10})$.

Let us rewrite the displacement vectors $u_1(x, z)$ and $w_1(x, z)$ using Fourier integral transforms as follows:

$$u_1(x, z) = \int_{-\infty}^{\infty} \tilde{u}_1(\alpha, z) e^{-I\alpha x} d\alpha \quad (7a)$$

$$w_1(x, z) = \int_{-\infty}^{\infty} \tilde{w}_1(\alpha, z) e^{-I\alpha x} d\alpha \quad (7b)$$

where $\tilde{u}_1(\alpha, z)$ and $\tilde{w}_1(\alpha, z)$ are the inverse Fourier transforms of the displacement vectors, α and I denote the transform variables and the imaginary unit, respectively.

Inserting Eq. (7) into the governing Eq. (6) and applying inverse Fourier transform gives rise to a system of ordinary differential equations

$$C_{55}^0 \frac{d^2 \tilde{u}_1}{dz^2} + \gamma C_{55}^0 \frac{d\tilde{u}_1}{dz} + \alpha^2 (-C_{11}^0 + c_1^2) \tilde{u}_1 - I\alpha (C_{13}^0 + C_{55}^0) \frac{d\tilde{w}_1}{dz} - I\alpha \gamma C_{55}^0 \tilde{w}_1 = 0 \quad (8a)$$

$$-I\alpha (C_{13}^0 + C_{55}^0) \frac{d\tilde{u}_1}{dz} - I\alpha \gamma C_{13}^0 \tilde{u}_1 + C_{33}^0 \frac{d^2 \tilde{w}_1}{dz^2} + \gamma C_{33}^0 \frac{d\tilde{w}_1}{dz} + \alpha^2 (-1 + c_1^2) C_{55}^0 \tilde{w}_1 = 0 \quad (8b)$$

The characteristic polynomial of the ordinary differential Eq. (8) is as

$$n^4 + L_1 n^3 + L_2 n^2 + L_3 n + L_4 = 0 \quad (9)$$

where

$$L_1 = 2\gamma \quad (10a)$$

$$L_2 = \frac{((C_{13}^0)^2 - C_{11}^0 C_{33}^0 + 2C_{13}^0 C_{55}^0)\alpha^2 + C_{55}^0 (c_1^2 (C_{33}^0 + C_{55}^0)\alpha^2 + C_{33}^0 \gamma^2)}{C_{33}^0 C_{55}^0} \quad (10b)$$

$$L_3 = \frac{((C_{13}^0)^2 - C_{11}^0 C_{33}^0 + 2C_{13}^0 C_{55}^0 + c_1^2 C_{55}^0 (C_{33}^0 + C_{55}^0))\alpha^2 \gamma}{C_{33}^0 C_{55}^0} \quad (10c)$$

$$L_4 = \frac{\alpha^2 ((-1 + c_1^2)(-C_{11}^0 \alpha^2 + c_1^2 C_{55}^0 \alpha^2) + C_{13}^0 \gamma^2)}{C_{33}^0} \quad (10d)$$

So, the solution of the system of ordinary differential Eq. (8) leads to the following transformed displacement expressions \tilde{u}_1 and \tilde{w}_1 :

$$\tilde{u}_1(\alpha, z) = \sum_{j=1}^4 A_j e^{n_j z}, \quad \tilde{w}_1(\alpha, z) = I \sum_{j=1}^4 m_j A_j e^{n_j z} \quad (11)$$

where n_j ($j = 1, 2, \dots, 4$) are the roots of the characteristic polynomial (9), A_j ($j = 1, 2, \dots, 4$) are the unknown functions which will be determined by the boundary conditions of the moving contact problem and m_j is found as

$$m_j = -\frac{I\alpha(C_{55}^0 n_j + C_{13}^0 (n_j + \gamma))}{(-1 + c_1^2)C_{55}^0 \alpha^2 + C_{33}^0 n_j (n_j + \gamma)} \quad (12)$$

Now, the stress expressions for the FG orthotropic layer can be rewritten by substituting Eq. (11) into Eq. (3):

$$\sigma_{x1}(x, z) = \frac{1}{2\pi} \int_{-\infty}^{\infty} \sum_{j=1}^4 [A_j (C_{13} m_j n_j - I\alpha C_{11}) e^{n_j z}] e^{-I\alpha x} d\alpha \quad (13a)$$

$$\sigma_{z1}(x, z) = \frac{1}{2\pi} \int_{-\infty}^{\infty} \sum_{j=1}^4 [A_j (C_{33} m_j n_j - I\alpha C_{13}) e^{n_j z}] e^{-I\alpha x} d\alpha \quad (13b)$$

$$\tau_{xz1}(x, z) = \frac{1}{2\pi} \int_{-\infty}^{\infty} \sum_{j=1}^4 [A_j C_{55} (n_j - I\alpha m_j) e^{n_j z}] e^{-I\alpha x} d\alpha \quad (13c)$$

Note that, by setting $C_{11}^0 = C_{33}^0 = \mu_2 \frac{\kappa_2 + 1}{\kappa_2 - 1}$, $C_{13}^0 = \mu_2 \frac{3 - \kappa_2}{\kappa_2 - 1}$, $C_{55}^0 = \mu_2$, $\gamma = 0$ and $h \rightarrow \infty$ the FG orthotropic layer becomes an homogeneous isotropic half plane. So, for isotropic half plane, the displacement and stress components can be given as [10]:

$$u_2(x, z) = \frac{1}{2\pi} \int_{-\infty}^{\infty} \sum_{j=1}^2 [B_j e^{n_{2j}\alpha z}] e^{-I\alpha x} d\alpha \quad (14a)$$

$$w_2(x, z) = \frac{1}{2\pi} \int_{-\infty}^{\infty} I \left[B_1 \frac{1}{n_{21}} e^{n_{21}\alpha z} + B_2 n_{22} e^{n_{22}\alpha z} \right] e^{-I\alpha x} d\alpha \quad (14b)$$

$$\sigma_{x2}(x, z) = \frac{1}{2\pi} \int_{-\infty}^{\infty} -I\mu_2 \alpha \left[2B_1 e^{n_{21}\alpha z} + B_2 \frac{(1 + n_{22}^2(-3 + \kappa_2) + \kappa_2)}{-1 + \kappa_2} e^{n_{22}\alpha z} \right] e^{-I\alpha x} d\alpha \quad (14c)$$

$$\sigma_{z2}(x, z) = \frac{1}{2\pi} \int_{-\infty}^{\infty} I\mu_2 \alpha \left[2B_1 e^{n_{21}\alpha z} + B_2 \frac{(-3 + n_{22}^2(1 + \kappa_2) + \kappa_2)}{-1 + \kappa_2} e^{n_{22}\alpha z} \right] e^{-I\alpha x} d\alpha \quad (14d)$$

$$\tau_{xz2}(x, z) = \frac{1}{2\pi} \int_{-\infty}^{\infty} \mu_2 \alpha \left[\frac{1 + n_{21}^2}{n_{21}} B_1 e^{n_{21}\alpha z} + 2n_{22} B_2 e^{n_{22}\alpha z} \right] e^{-I\alpha x} d\alpha \quad (14e)$$

where $\kappa_2 = 3 - 4\nu_2$. Also μ_2 is the shear modulus and ν_2 is the Poisson's ratio of the isotropic half plane, respectively. B_j ($j = 1, 2$) are the unknowns which will be determined from the boundary conditions of the problem. n_{2j} ($j = 1, 2$) is defined as

$$n_{21} = \sqrt{1 - c_2^2}, \quad n_{22} = \sqrt{1 - c_2^2 \frac{(-1 + \kappa_2)}{(1 + \kappa_2)}} \quad (15)$$

where $c_2 = V/\sqrt{\mu_2/\rho_2}$.

Note that, in a translating coordinate system, the unknowns A_j ($j = 1, 2 \dots 4$), B_1 and B_2 will be determined with the help of boundary and continuity conditions (1).

3 Derivation of singular integral equation

In this section, we will use the basic equations of elasticity theory and boundary conditions (1) to derive the singular integral equation. Using Eqs. (13)–(14) in the boundary conditions (1) and applying inverse Fourier transform, six linear algebraic equations are obtained. By solving the obtained system of linear algebraic equations, the coefficients A_j and B_j can be obtained depending on the unknown contact stress $p(x)$ as the following form

$$A_j = \int_{-a}^b p(\xi) e^{I\alpha\xi} (A_j^p + \eta A_j^q) d\xi \quad j = 1, 2 \dots 4 \quad (16a)$$

$$B_j = \int_{-a}^b p(\xi) e^{I\alpha\xi} (B_j^p + \eta B_j^q) d\xi \quad j = 1, 2 \quad (16b)$$

The following mixed condition will be used to find the unknown contact stress $p(x)$

$$\frac{\partial w_1(x, 0)}{\partial x} = \frac{x}{R} \quad (17)$$

Using the unknowns A_j in the mixed condition (17) and considering the asymptotic behavior of the kernels for $|\alpha| \rightarrow \infty$ yields the following second kind of singular integral equation of Cauchy type:

$$\eta\phi_2 p(x) + \frac{1}{\pi} \int_{-a}^b p(\xi) \left[\frac{\phi_1}{\xi - x} + K_1(x, \xi) + \eta K_2(x, \xi) \right] d\xi = \frac{x}{R} \quad (-a < x < b) \quad (18)$$

where

$$K_1(x, \xi) = \int_0^\infty (S_1(\alpha) - \phi_1) \sin \alpha(\xi - x) d\alpha \quad (19a)$$

$$K_2(x, \xi) = \int_0^\infty (S_2(\alpha) - \phi_2) \cos \alpha(\xi - x) d\alpha \quad (19b)$$

$$S_1(\alpha) = \alpha \sum_{j=1}^4 A_j^p m_j, \quad S_2(\alpha) = -I\alpha \sum_{j=1}^4 A_j^q m_j \quad (19c)$$

$$\phi_1 = \lim_{\alpha \rightarrow \infty} S_1(\alpha), \quad \phi_2 = \lim_{\alpha \rightarrow \infty} S_2(\alpha) \quad (19d)$$

Note that, the contact widths must satisfy the following equilibrium condition

$$\int_{-\infty}^\infty \sigma_{z1}(x, 0) dx = - \int_{-a}^b p(\xi) d\xi = -P \quad (20)$$

4 Numerical solution of the singular integral equation

This section presents the numerical solution of the singular integral Eq. (18). Here, it is aimed to convert the solution of singular integral equation to the solution of system of algebraic equations. Gauss–Jacobi integration formulas are used to approach the numerical solution. So, first, the singular integral equation should be converted to the dimensionless form by using following normalization procedure:

$$\xi = \frac{a+b}{2}r + \frac{b-a}{2}, \quad x = \frac{a+b}{2}s + \frac{b-a}{2} \quad (21)$$

Hence, the integral Eq. (18) can be rewritten as

$$\eta\phi_2 p(s) + \frac{1}{\pi} \int_{-1}^1 p(r) \left[\frac{\phi_2}{r-s} + K_1^*(s, r) + \eta K_2^*(s, r) \right] dr = f(s) \quad (22)$$

where

$$K_1^*(s, r) = \frac{a+b}{2} K_1(x, \xi), \quad K_2^*(s, r) = \frac{a+b}{2} K_2(x, \xi), \quad f(s) = \frac{1}{R} \left(\frac{a+b}{2}s + \frac{b-a}{2} \right) \quad (23)$$

By applying the same variable transform (21) to the equilibrium condition (20), the following integral equation can be obtained:

$$\frac{a+b}{2} \int_{-1}^1 p(r) dr = P \quad (24)$$

Since the punch profile is cylindrical, smooth contact occurs at the end points of the contact $x = -a$ and $x = b$. Therefore, the index of the integral Eq. (18) is taken -1 .

Now, let us seek the solution of the singular integral Eq. (22) as

$$p(r) = g(r)(1-r)^{\beta_1}(1+r)^{\beta_2} \quad (25)$$

where $g(r)$ is an unknown bounded function and

$$\beta_1 = \frac{1}{2\pi I} \ln \left[\frac{\eta\phi_2/\phi_1 - I}{\eta\phi_2/\phi_1 + I} \right] \quad (26a)$$

$$\beta_2 = -\frac{1}{2\pi I} \ln \left[\frac{\eta\phi_2/\phi_1 - I}{\eta\phi_2/\phi_1 + I} \right] + 1 \quad (26b)$$

By applying Gauss–Jacobi integration formulas [38] to the singular integral Eq. (22) and equilibrium condition (24), the following system of algebraic equations is obtained:

$$\sum_{i=1}^N W_i^N g(r_i) \left[\frac{1}{r_i - s_k} + K_1^*(s_k, r_i) + \eta K_2^*(s_k, r_i) \right] = f(s_k) \quad k = 1, 2, \dots, N+1 \quad (27)$$

$$\frac{b+a}{2} \sum_{i=1}^N W_i^N g(r_i) = \frac{P}{\pi} \quad (28)$$

where r_i and s_k are the roots of Jacobi polynomials defined as

$$P_N^{(\alpha, \beta)}(r_i) = 0 \quad i = 1, 2, \dots, N \quad (29a)$$

$$P_{N+1}^{(-\alpha, -\beta)}(s_k) = 0 \quad k = 1, 2, \dots, N+1 \quad (29b)$$

and W_i^N is the weighting constant given as follows:

$$W_i^N = -\frac{1}{\pi} \frac{2N + \alpha + \beta}{(N+1)!} \frac{\Gamma(N + \alpha + 1)\Gamma(N + \alpha + 1)}{\Gamma(N + \alpha + \beta + 1)} \frac{2^{(\alpha+\beta)}}{P_N^{(\alpha, \beta)'}(r_i)P_{N+1}^{(\alpha, \beta)}(r_i)} \quad (29c)$$

Table 1 Material properties of glass/epoxy [39]

C_{ij}	(GPa)	C_{ij}	(GPa)
C_{11}	46.86	C_{32}	10.49
C_{12}	77.04	C_{33}	18.04
C_{13}	77.04	C_{44}	3.78
C_{21}	77.04	C_{55}	8.24
C_{22}	18.04	C_{66}	8.24
C_{23}	10.49	E_{xx}	42.70
C_{31}	77.04		

As is seen from Eqs. (27) and (28), there are $N + 2$ equations which have $N + 2$ unknowns. The unknowns are $g(r_i)$ ($i = 1, 2, \dots, N$) and contact widths a and b . Since the contact widths a and b are initially unknown, the system of equations is non-linear, and, therefore, an iterative procedure is applied to determine the contact widths. In the iterative algorithm the initial values of the a and b are chosen and N unknowns $g(r_i)$ are determined from the linear algebraic equations in (27). Then, the subtracted equation in (27), i.e. the consistency condition and the equilibrium condition (25) are checked. If the selected accuracy is not achieved, new values of a and b are selected. The selection of new values of a and b will continue until a and b achieve the desired accuracy.

In mechanics, the analysis of in-plane stress is also an important subject. The in-plane stress at the surface of FG orthotropic layer $\sigma_{x1}(x, 0)$ can be determined by the relation below:

$$\sigma_{x1}(x, 0) = \begin{cases} \phi_3 p(x) + H(x), & -a < x < b \\ H(x), & x \leq -a, x \geq b \end{cases} \quad (30)$$

where

$$H(x) = \frac{1}{\pi} \int_{-a}^b p(\xi) \left[\phi_4 \frac{\eta}{\xi - x} + K_3(x, \xi) + \eta K_4(x, \xi) \right] d\xi \quad (31a)$$

$$K_3(x, \xi) = \int_0^{\infty} (S_3(\alpha) - \phi_3) \cos \alpha(\xi - x) d\alpha \quad (31b)$$

$$K_4(x, \xi) = \int_0^{\infty} (S_4(\alpha) - \phi_4) \sin \alpha(\xi - x) d\alpha \quad (31c)$$

$$S_3(\alpha) = \sum_{j=1}^4 \left[A_j^p (C_{13} m_j n_j - I \alpha C_{11}) \right] \quad (31d)$$

$$S_4(\alpha) = I \sum_{j=1}^4 \left[A_j^q (C_{13} m_j n_j - I \alpha C_{11}) \right] \quad (31e)$$

$$\phi_3 = \lim_{\alpha \rightarrow \infty} S_3(\alpha), \quad \phi_4 = \lim_{\alpha \rightarrow \infty} S_4(\alpha) \quad (31f)$$

5 Numerical results

This section presents the effect of the dimensionless quantities such as moving velocity $V^* = V/\sqrt{C_{55}^0/\rho_{10}}$, inhomogeneity parameter $\Gamma = C_h/C_0$, friction coefficient η , shear modulus of the half plane $\mu_2^* = \mu_2/C_{55}^0$, density of the half plane $\rho_2^* = \rho_2/\rho_{10}$ and indentation load $P^* = P/(C_{55}^0 h)$, on the dimensionless contact stress $p(x)/C_{55}^0$ and in-plane stress $\sigma_{x1}(x, 0)/C_{55}^0$ are given. During the analysis, it is assumed that the FG orthotropic layer is made of glass/epoxy (GI/Ep). The material properties of glass/epoxy are listed in Table 1.

By setting $\Gamma = C_h/C_0 = 1$ the FG orthotropic layer becomes a homogeneous orthotropic layer. So, it gives a chance to validate the present results with the numerical results obtained in [20]. As a result of comparison of the results of the limiting case by [20], a very good agreement was obtained as depicted in Fig. 2.

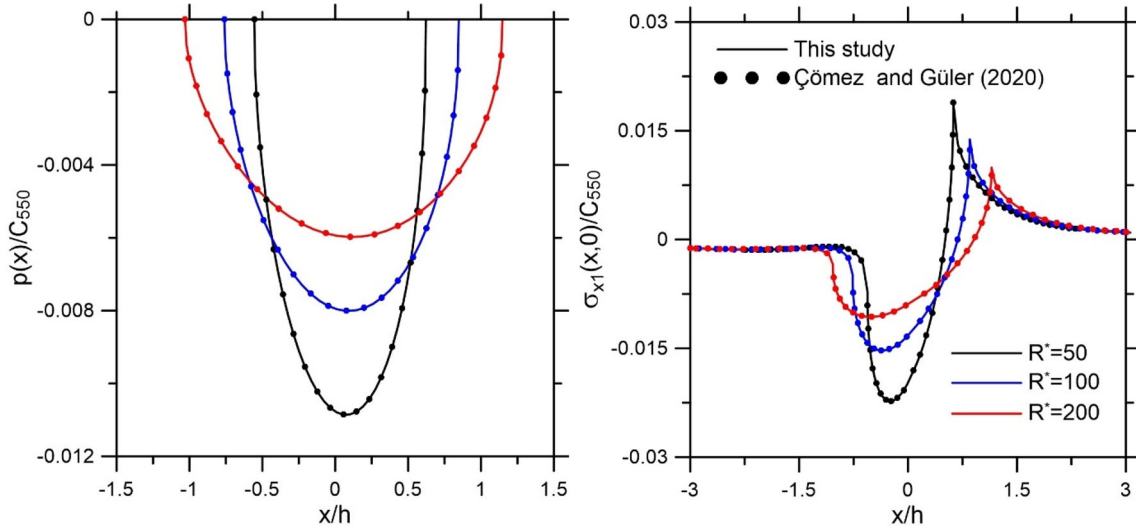


Fig. 2 Comparison of the contact stress and in-plane stress with those from [20]. ($V^* = 0.4$, $\eta = 0.4$, $P/(C_{550}h) = 0.01$, $\Gamma = C_h/C_0 = 1$, $\rho_2/\rho_{10} = 1$, $\mu_2/C_{550} = 2$)

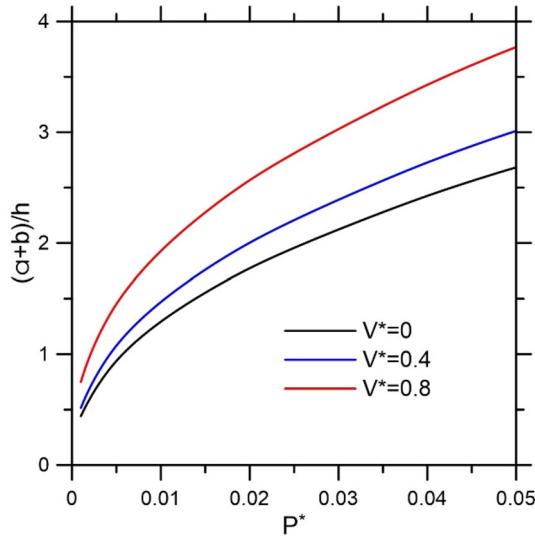


Fig. 3 Variation of the contact width $(a + b)/h$ with moving velocity V^* and indentation load P^* . ($\eta = 0.4$, $R/h = 100$, $\Gamma = C_h/C_0 = 2$, $\rho_2/\rho_{10} = 1.5$, $\mu_2/C_{550} = 2$)

Variation of the contact width with moving velocity V^* and indentation load P^* is given in Fig. 3. It is seen in the figure that the punch becomes more embedded in the layer with increasing load. On the other hand, increasing the movement speed at small load values affects the contact width less than at large load values.

Variation of the contact width with the shear modulus of the half-plane and Γ inhomogeneity parameter is shown in Fig. 4. The stiffness of the functionally graded orthotropic layer changes exponentially depending on the Γ inhomogeneity parameter, starting from the bottom surface of the layer. Increasing the Γ parameter increases the stiffness of the FG layer while decreasing the Γ parameter reduces the stiffness of the FG layer. The situation where Γ is equal to one corresponds to the homogeneous layer particular case. When the layer become soft, the penetration between the punch and the layer increases, and, accordingly, the contact width between the FG layer and the punch increases. At values of the Γ inhomogeneity parameter close to zero, there is a tendency for contact widths to approach infinity. On the other hand, as the dimensionless shear modulus ratio of the half-plane decreases, the contact widths under the punch increase as the half-plane becomes flexible. Especially if this ratio is equal to 0.5, contact widths increase significantly.

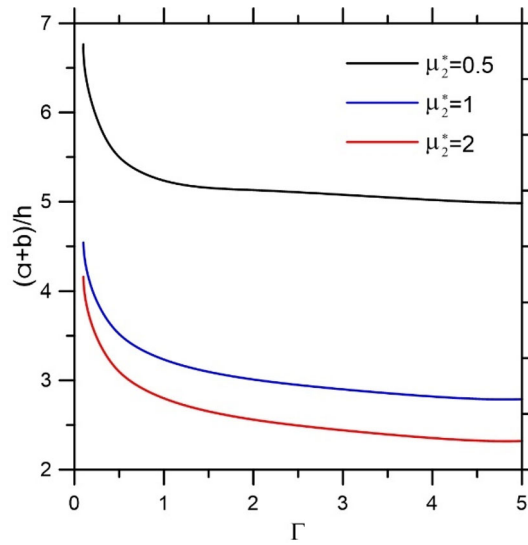


Fig. 4 Variation of the contact width $(a + b)/h$ with shear modulus of half plane μ_2^* and inhomogeneity parameter Γ . ($\eta = 0.4$, $R/h = 200$, $P/(C_{550}h) = 0.02$, $\rho_2/\rho_{10} = 2$, $V^* = 0.2$)

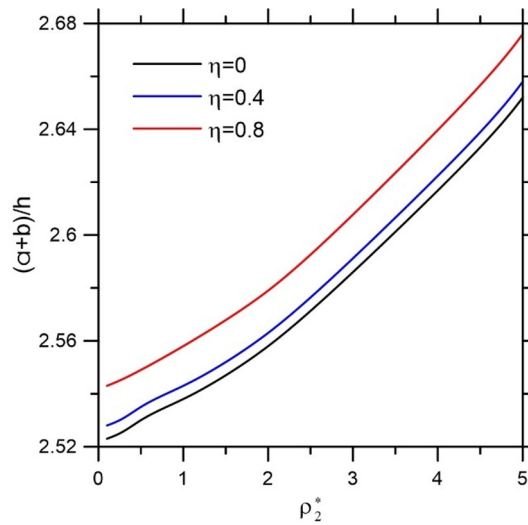


Fig. 5 Variation of the contact width $(a + b)/h$ with friction coefficient η and density of half plane ρ_2^* . ($R/h = 200$, $P/(C_{550}h) = 0.02$, $\Gamma = C_h/C_0 = 2$, $V^* = 0.2$, $\mu_2/C_{550} = 2$)

Figure 5 shows the variation of the contact width with the friction coefficient η and dimensionless density of the half-plane ρ_2^* . It can be concluded from the figure that changes in density ratio and friction coefficient do not much affect the contact width. On the other hand, since it creates resistance forces that prevent separation between the FG layer and the punch due to the friction forces, it causes a slight decrease in the contact widths between the punch and the FG layer. Moreover, according to Newton's law of motion, as the mass density increases, the dynamic forces acting on the system due to the speed of the punch also increase. Therefore, as the density ratio ρ_2^* increases, the contact lengths under the punch increase slightly.

Figure 6 presents the variation of the dimensionless contact stress and in-plane stress versus different moving velocity values. The regions where tensile stress occurs in the $\sigma_{x1}(x, 0)/C_{55}^0$ in-plane stress distribution under the punch are the regions where contact damage and crack formation are likely. Surface cracks may subsequently cause fatigue cracks to form and propagate. For this reason, the dimensionless $\sigma_{x1}(x, 0)/C_{55}^0$ in-plane stress distribution under the punch was evaluated based on the behavior of tensile stresses. As can be seen from the figure, because of the increase in the moving speed of the punch, the peak value of the tensile

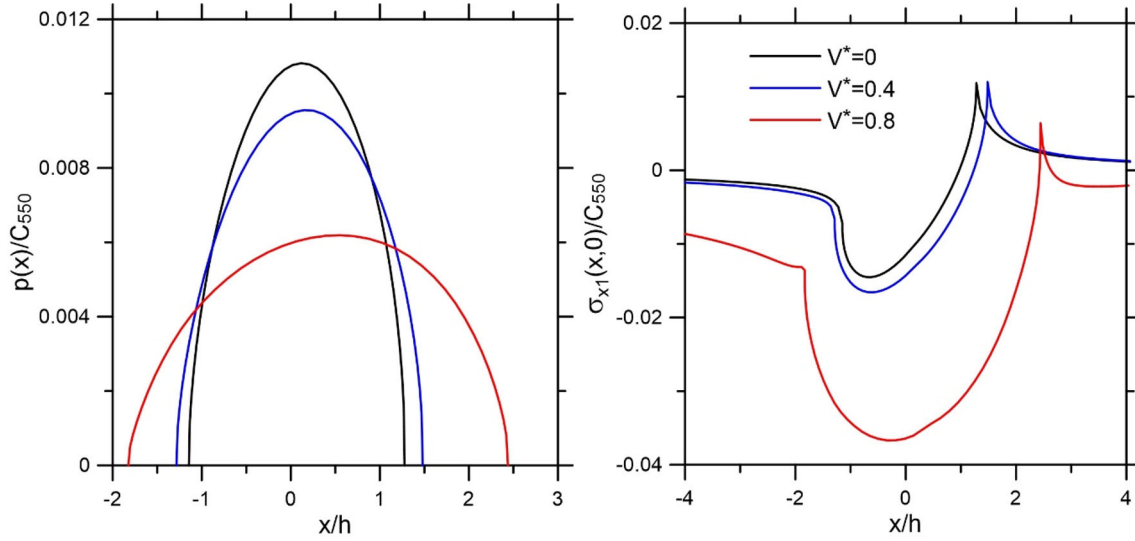


Fig. 6 Variations of the contact stress, $p(x)$, in-plane stress, $\sigma_{x1}(x, 0)$, versus moving velocity, V^* . ($R/h = 200$, $P/(C_{550}h) = 0.02$, $\Gamma = C_h/C_0 = 2$, $\rho_2/\rho_{10} = 2$, $\mu_2/C_{550} = 2$)

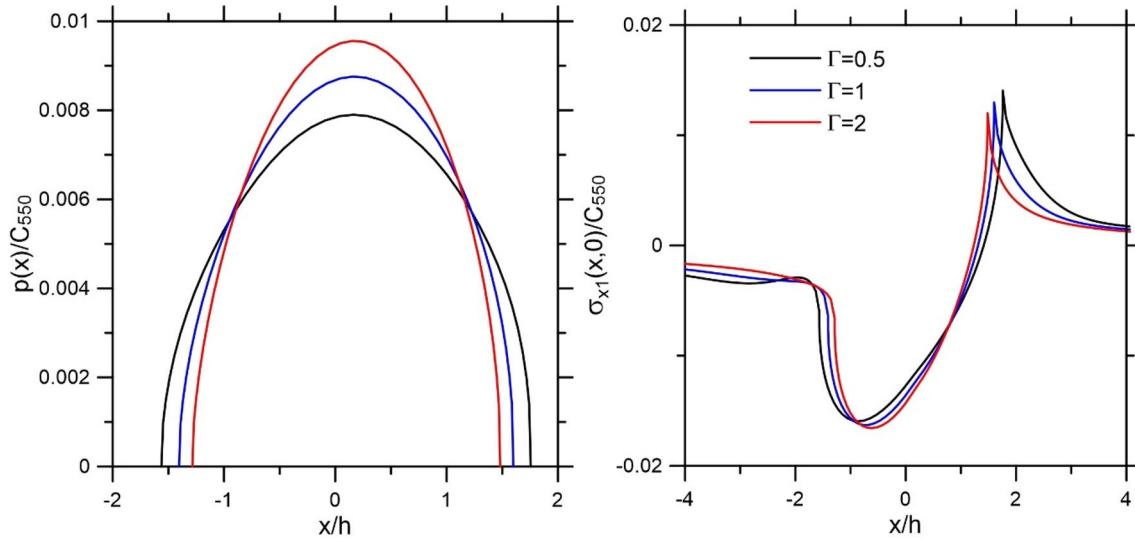


Fig. 7 Variations of the contact stress, $p(x)$, in-plane stress, $\sigma_{x1}(x, 0)$, versus inhomogeneity parameter, Γ . ($\eta = 0.4$, $R/h = 200$, $P/(C_{550}h) = 0.02$, $\rho_2/\rho_{10} = 2$, $V^* = 0.4$, $\mu_2/C_{550} = 2$)

stresses in the $\sigma_{x1}(x, 0)/C_{55}^0$ in-plane stress distribution decreases. In addition, it leads to smaller contact pressure associated with a larger contact zone when the punch slides faster.

Variations of the contact stress $p(x)/C_{55}^0$ and in-plane stress $\sigma_{x1}(x, 0)/C_{55}^0$ versus inhomogeneity parameter Γ are illustrated in Fig. 7. As can be seen from the figure, as the Γ inhomogeneity parameter increases, the FG layer will become stiffer and the dimensionless contact widths under the punch decrease. Since the stresses will disperse over a smaller area, the maximum value of the contact stresses under the punch increases. Although the $\sigma_{x1}(x, 0)/C_{55}^0$ in-plane stresses under the punch are not significantly affected by the increase in this Γ inhomogeneity parameter, the peak value of the tensile stresses at the trailing edge decreases slightly.

Figure 8 presents variations of contact stress $p(x)/C_{55}^0$ and in-plane stress $\sigma_{x1}(x, 0)/C_{55}^0$ versus friction coefficient η . The distribution of dimensionless contact stresses under the punch is symmetrical in the case of frictionless contact ($\eta = 0$) and takes its largest value on the z-axis. This symmetry disappears when friction forces are influential ($\eta \neq 0$). However, as the friction forces increase, the values of the tensile stresses at the right end of the distribution of dimensionless $\sigma_{x1}(x, 0)/C_{55}^0$ in-plane normal stresses increase significantly.

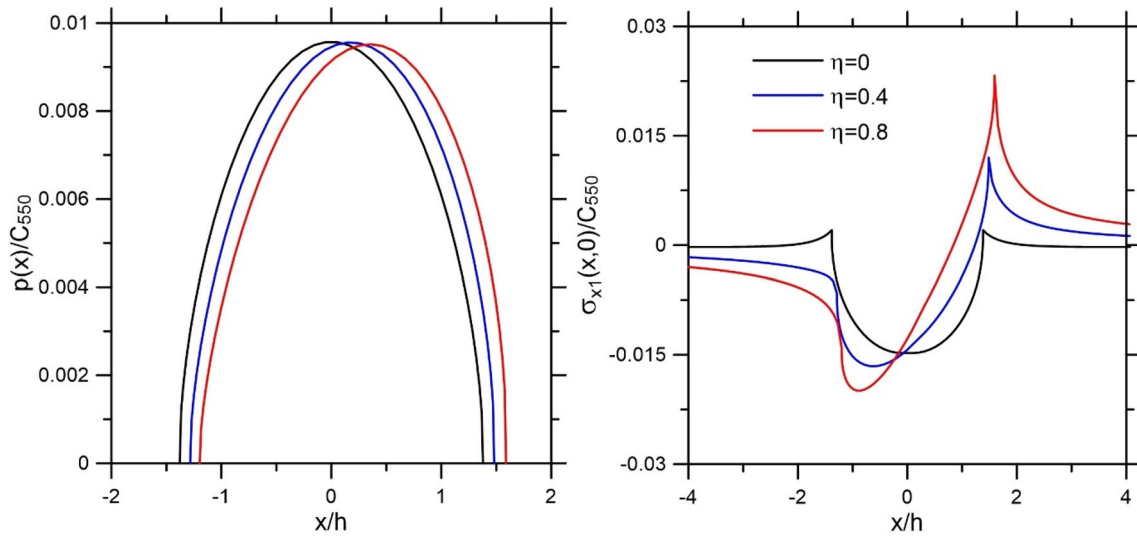


Fig. 8 Variations of the contact stress, $p(x)$, in-plane stress, $\sigma_{x1}(x, 0)$, versus friction coefficient, η . ($R/h = 200$, $P/(C_{550}h) = 0.02$, $\Gamma = C_h/C_0 = 2$, $\rho_2/\rho_{10} = 2$, $V^* = 0.4$, $\mu_2/C_{550} = 2$)

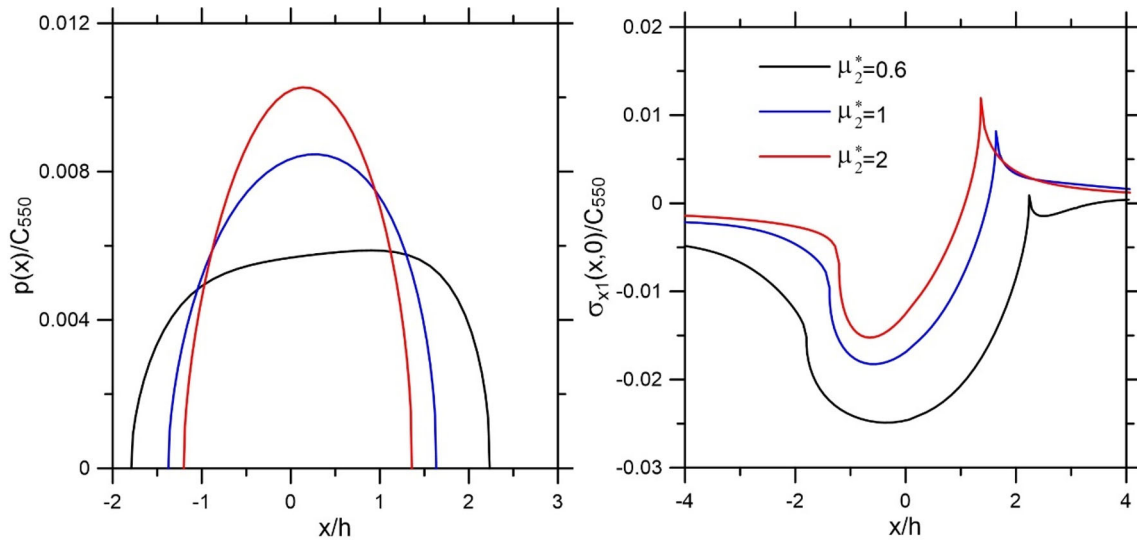


Fig. 9 Variations of the contact stress, $p(x)$, in-plane stress, $\sigma_{x1}(x, 0)$, versus shear modulus of half plane, μ_2^* . ($\eta = 0.4$, $R/h = 200$, $P/(C_{550}h) = 0.02$, $\Gamma = C_h/C_0 = 2$, $\rho_2/\rho_{10} = 2$, $V^* = 0.2$)

Therefore, it should be taken into consideration that increased friction effects may cause damage and crack formation on the contact surfaces. To prevent such damage, a small coefficient of friction should be selected.

Figure 9 illustrates variations of contact stress $p(x)/C_{55}^0$ and in-plane stress $\sigma_{x1}(x, 0)/C_{55}^0$ versus the dimensionless shear modulus of the half-plane μ_2^* . Since the rigidity of the system increases with bigger values of μ_2^* ratio, the contact width under the punch decreases. Additionally, the maximum values of tensile stresses in the $\sigma_{x1}(x, 0)/C_{55}^0$ in-plane stress distribution increase with the increase in the shear modulus of the half-plane μ_2^* .

Variations of the contact stress $p(x)/C_{55}^0$ and in-plane stress $\sigma_{x1}(x, 0)/C_{55}^0$ versus indentation load P^* and dimensionless density of the half-plane ρ_2^* are shown in Fig. 10 and Fig. 11. In contrast to the other parameters, an increase in load increases both contact widths and contact stresses together. The peak values of tensile stresses in the $\sigma_{x1}(x, 0)/C_{55}^0$ in-plane stress distribution under the punch also increase significantly with this increase. Although the change in the dimensionless density values of the half-plane ρ_2^* does not have

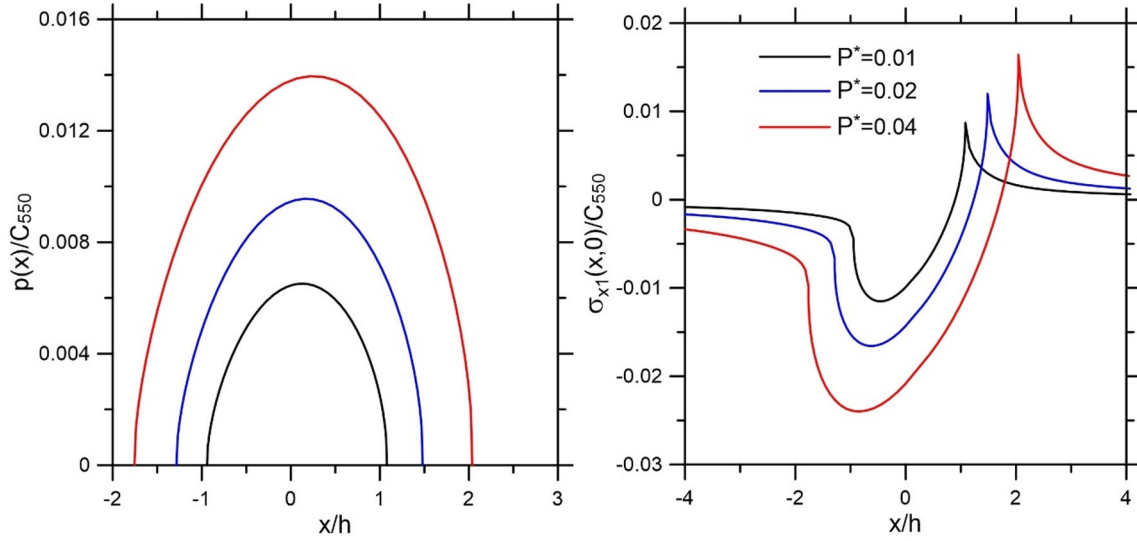


Fig. 10 Variations of the contact stress, $p(x)$, in-plane stress, $\sigma_{x1}(x, 0)$, versus indentation load, P^* . ($\eta = 0.4$, $R/h = 200$, $\Gamma = C_h/C_0 = 2$, $\rho_2/\rho_{10} = 2$, $V^* = 0.4$, $\mu_2/C_{550} = 2$)

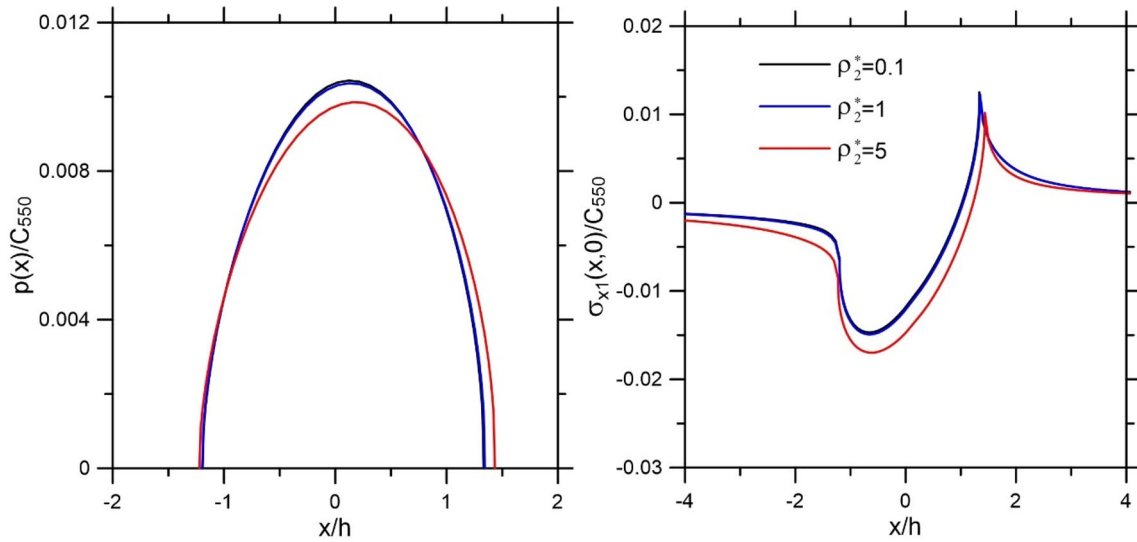


Fig. 11 Variations of the contact stress, $p(x)$, in-plane stress, $\sigma_{x1}(x, 0)$, versus density of half plane, ρ_2^* . ($\eta = 0.4$, $R/h = 200$, $P/(C_{550}h) = 0.02$, $\Gamma = C_h/C_0 = 2$, $V^* = 0.2$, $\mu_2/C_{550} = 2$)

a significant effect, the peak values of the contact stress under the punch and the $\sigma_{x1}(x, 0)/C_{55}^0$ in-plane tensile stresses decrease slightly as this value increases.

Figures 12 and 13 show the effect of C_{330} and C_{110} orthotropy constants on the distribution of $p(x)$ contact stress and $\sigma_{x1}(x, 0)$ in-plane stress. Since increasing the C_{330} orthotropy constant will increase the material rigidity in the direction of the force, the contact length under the punch decreases, and the peak value of contact stress increases for increasing the C_{330} orthotropy constant value. In the $\sigma_{x1}(x, 0)$ in-plane stresses under the punch, as the C_{330} orthotropy constant increases, the maximum value of the tensile stress, which can trigger crack formation and surface damage, also increases. The change of the C_{110} orthotropy constant is not related to the change of material stiffness in the force direction. However, since the increase in the C_{110} orthotropy constant will increase the layer stiffness, the contact lengths under the punch decrease slightly. Additionally, with the increase of the C_{110} orthotropy constant, the maximum value of in-plane $\sigma_{x1}(x, 0)$ tensile stress under the punch increases significantly.

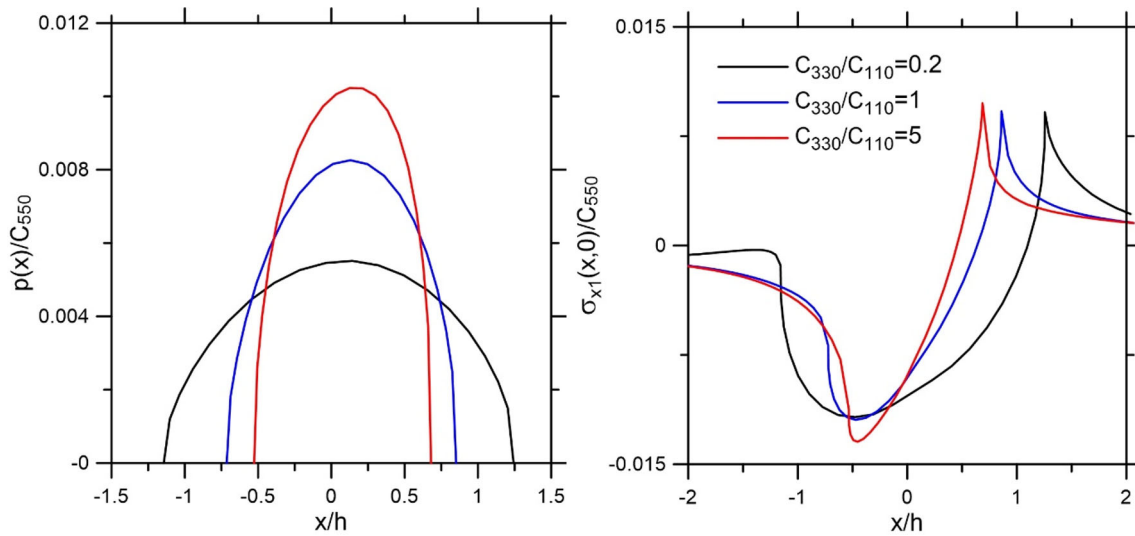


Fig. 12 Variations of the contact stress, $p(x)$, in-plane stress, $\sigma_{x1}(x, 0)$, versus orthotropy constant C_{330} . ($\eta = 0.4$, $R/h = 200$, $P/(C_{550}h) = 0.01$, $\Gamma = C_h/C_0 = 2$, $\rho_2/\rho_{10} = 1$, $V^* = 0.4$, $\mu_2/C_{550} = 2$)

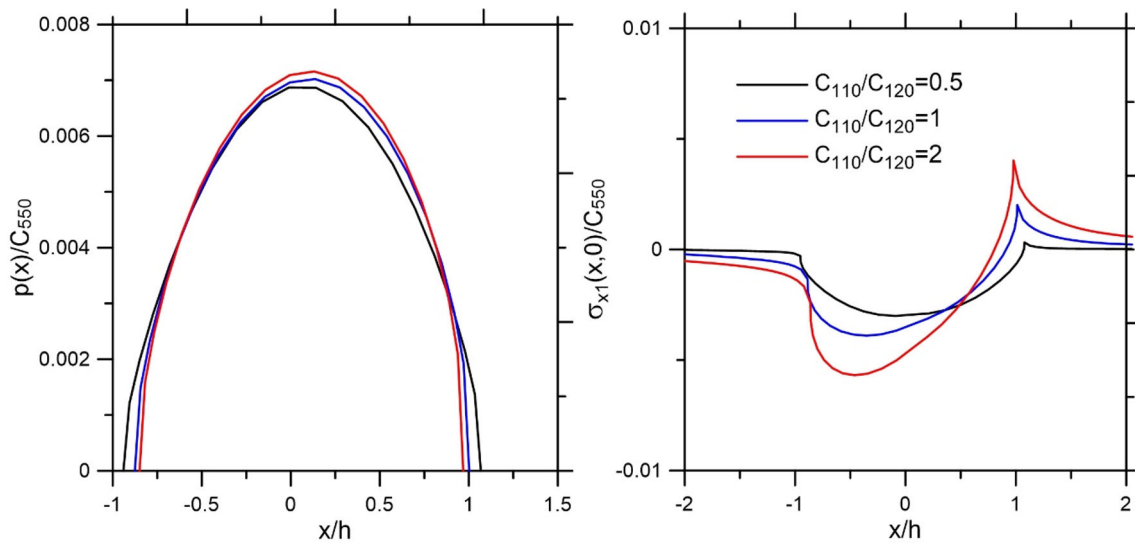


Fig. 13 Variations of the contact stress, $p(x)$, in-plane stress, $\sigma_{x1}(x, 0)$, versus orthotropy constant C_{110} . ($\eta = 0.4$, $R/h = 200$, $P/(C_{550}h) = 0.01$, $\Gamma = C_h/C_0 = 2$, $\rho_2/\rho_{10} = 1$, $V^* = 0$, $\mu_2/C_{550} = 2$)

6 Conclusions

This study investigated the moving contact problem of a functionally graded orthotropic-coated half-plane. Numerical results for dimensionless contact widths, contact pressures and in-plane stress distributions under the punch were obtained for different values of moving velocity, indentation loads, inhomogeneity parameter, the density of the half-plane, shear modulus of the half-plane and friction coefficient. The outcomes of the study can be summarized as given as follows.

- Dimensionless contact widths under the punch vary directly proportional to the moving velocity, indentation load, and orthotropy constant C_{330} , and inversely proportional to the values of the inhomogeneity parameter and the dimensionless shear modulus of the half plane. The size of the contact area under the punch is not much affected by the change in the friction coefficient, the dimensionless density ratio of the half plane and orthotropy constant C_{110} .
- The regions where tensile stress occurs at the in-plane stress distribution under the punch are the regions where contact damage and crack formation are likely. Surface cracks may subsequently cause fatigue cracks

to form and propagate. In the $\sigma_{x1}(x, 0)/C_{55}^0$ in-plane stress distribution, the peak values of tensile stresses increase significantly with the increase in the friction coefficient, dimensionless shear modulus of the half-plane, indentation load values, orthotropy constants C_{110} and C_{330} . On the other hand, increasing the moving velocity of the punch causes the peak values of tensile stresses to decrease. The change in the density ratio of the half-plane and the Γ inhomogeneity parameter values does not have much effect on the peak values of tensile stresses.

Funding Open access funding provided by the Scientific and Technological Research Council of Türkiye (TÜBİTAK). No funding was received for conducting this study.

Declarations

Conflict of interest The authors have no relevant financial or non-financial interests to disclose.

Open Access This article is licensed under a Creative Commons Attribution 4.0 International License, which permits use, sharing, adaptation, distribution and reproduction in any medium or format, as long as you give appropriate credit to the original author(s) and the source, provide a link to the Creative Commons licence, and indicate if changes were made. The images or other third party material in this article are included in the article's Creative Commons licence, unless indicated otherwise in a credit line to the material. If material is not included in the article's Creative Commons licence and your intended use is not permitted by statutory regulation or exceeds the permitted use, you will need to obtain permission directly from the copyright holder. To view a copy of this licence, visit <http://creativecommons.org/licenses/by/4.0/>.

References

1. Suresh, S., Mortensen, A.: *Fundamentals of Functionally Graded Materials: Processing and Thermomechanical Behaviour of Graded Metals and Metal-Ceramic Composites*. IOM Communications, London (1998)
2. Chen, P., Chen, S.: Thermo-mechanical contact behavior of a finite graded layer under a sliding punch with heat generation. *Int. J. Solids Struct.* **50**(7–8), 1108–1119 (2013)
3. Guler, M.A., Erdogan, F.: The frictional sliding contact problems of rigid parabolic and cylindrical stamps on graded coatings. *Int. J. Mech. Sci.* **49**(2), 161–182 (2007)
4. Draiche, K., Bousahla, A.A., Tounsi, A., Hussain, M.: An integral shear and normal deformation theory for bending analysis of functionally graded sandwich curved beams. *Arch. Appl. Mech.* **91**, 4669–4691 (2021)
5. Yang, Y., Lam, C.C., Kou, K.P., Iu, V.P.: Free vibration analysis of the functionally graded sandwich beams by a meshfree boundary-domain integral equation method. *Compos. Struct.* **117**, 32–39 (2014)
6. Yang, Y., Kou, K.P., Iu, V.P., Lam, C.C., Zhang, C.: Free vibration analysis of two-dimensional functionally graded structures by a meshfree boundary-domain integral equation method. *Compos. Struct.* **110**, 342–353 (2014)
7. Rezaiee-Pajand, M., Arabi, E., Masoodi, A.R.: Nonlinear analysis of FG-sandwich plates and shells. *Aerosp. Sci. Technol.* **87**, 178–189 (2019)
8. Xu, X.J., Meng, J.M.: A model for functionally graded materials. *Compos. B Eng.* **145**, 70–80 (2018)
9. Chikh, A.: Investigations in static response and free vibration of a functionally graded beam resting on elastic foundations. *Frattura ed Integrità Strutturale* **14**(51), 115–126 (2020)
10. Galin, L.A.: *Contact Problems: The Legacy of LA Galin* (Vol. 155). Springer (2008)
11. Balci, M.N., Dag, S.: Dynamic frictional contact problems involving elastic coatings. *Tribol. Int.* **124**, 70–92 (2018)
12. Balci, M.N., Dag, S.: Mechanics of dynamic contact of coated substrate and rigid cylindrical ended punch. *J. Mech. Sci. Technol.* **33**, 2225–2240 (2019)
13. Balci, M.N., Dag, S.: Moving contact problems involving a rigid punch and a functionally graded coating. *Appl. Math. Model.* **81**, 855–886 (2020)
14. Balci, M.N., Dag, S.: Solution of the dynamic frictional contact problem between a functionally graded coating and a moving cylindrical punch. *Int. J. Solids Struct.* **161**, 267–281 (2019)
15. Zhou, Y.T., Lee, K.Y., Jang, Y.H.: Indentation theory on orthotropic materials subjected to a frictional moving punch. *Arch. Mech.* **66**(2), 71–94 (2014)
16. Zhou, Y.T., Lee, K.Y., Jang, Y.H.: Explicit solution of the frictional contact problem of anisotropic materials indented by a moving stamp with a triangular or parabolic profile. *Z. Angew. Math. Phys.* **64**, 831–861 (2013)
17. Zhou, Y.T., Lee, K.Y.: Dynamic behavior of a moving frictional punch over the surface of anisotropic materials. *Appl. Math. Model.* **38**(9–10), 2311–2327 (2014)
18. Çömez, İ.: Contact problem for a functionally graded layer indented by a moving punch. *Int. J. Mech. Sci.* **100**, 339–344 (2015)
19. Çömez, İ.: Frictional moving contact problem for a layer indented by a rigid cylindrical punch. *Arch. Appl. Mech.* **87**, 1993–2002 (2017)
20. Çömez, İ., Güler, M.A.: On the contact problem of a moving rigid cylindrical punch sliding over an orthotropic layer bonded to an isotropic half plane. *Math. Mech. Solids* **25**(10), 1924–1942 (2020)
21. Çömez, İ.: Sliding moving contact problem between a rigid cylindrical punch and a functionally graded orthotropic layer bonded to an isotropic homogeneous layer. *Mech. Based Des. Struct. Mach.*, 1–14 (2022)

22. Zhou, Y.T., Kim, T.W.: Frictional moving contact over the surface between a rigid punch and piezomagnetic materials—Terfenol-D as example. *Int. J. Solids Struct.* **50**(24), 4030–4042 (2013)
23. Bagheri, R., Ayatollahi, M., Rahmani, O.: Multiple moving cracks in a nonhomogeneous orthotropic strip. *Iran. J. Mech. Eng. Trans. ISME* **14**(1), 17–32 (2013)
24. Bagheri, R., Hosseini, S.M.: Multiple moving cracks in a non-homogeneous orthotropic plane. *J. Environ. Friendly Mater.* **5**(1), 29–34 (2021)
25. Hashemi, S.M.M., Ayatollahi, M.: Transient behavior of an orthotropic layer with imperfect FGM coating containing multiple interfacial and embedded cracks under anti-plane shear impact load. *Mech. Mater.* **164**, 104119 (2022)
26. Mottale, H., Monfared, M.M., Bagheri, R.: The multiple parallel cracks in an orthotropic non-homogeneous infinite plane subjected to transient in-plane loading. *Eng. Fract. Mech.* **199**, 220–234 (2018)
27. Lei, J., Xu, Y., Gu, Y., Fan, C.M.: The generalized finite difference method for in-plane crack problems. *Eng. Anal. Bound. Elem.* **98**, 147–156 (2019)
28. Yusufoglu, E., Turhan, I.: A mixed boundary value problem in orthotropic strip containing a crack. *J. Frankl. Inst.* **349**(9), 2750–2769 (2012)
29. Yusufoglu, E., Turhan, I.: A numerical approach for a crack problem by Gauss–Chebyshev quadrature. *Arch. Appl. Mech.* **83**, 1535–1547 (2013)
30. Erbas, B., Yusufoglu, E., Kaplunov, J.: A plane contact problem for an elastic orthotropic strip. *J. Eng. Math.* **70**, 399–409 (2011)
31. Rodríguez-Tembleque, L., Abascal, R.: Fast FE–BEM algorithms for orthotropic frictional contact. *Int. J. Numer. Meth. Eng.* **94**(7), 687–707 (2013)
32. Pozharskii, D.A.: Contact problem for an orthotropic half-space. *Mech. Solids* **52**(3), 315–322 (2017)
33. Hakobyan, V.N., Dashtoyan, L.L.: Contact problem for an orthotropic plane with a slit. *Mech. Compos. Mater.* **49**, 507–518 (2013)
34. Shavlakadze, N., Odishelidze, N., Criado-Aldeanueva, F.: The adhesive contact problem for a piecewise-homogeneous orthotropic plate with an elastic patch. *Math. Mech. Solids* **28**(8), 1798–1808 (2023)
35. Hou, P.F., Jiang, H.Y., Li, J.R.: A method for the orthotropic coating-substrate system: Green’s function for a normal line force on the surface. *Int. J. Mech. Sci.* **96**, 172–181 (2015)
36. Ustinov, K.B., Idrisov, D.M.: On delamination of bi-layers composed by orthotropic materials: exact analytical solutions for some particular cases. *ZAMM-J. Appl. Math. Mech./Z. für Angew. Math. und Mech.* **101**(4), e202000239 (2021)
37. Cao, R., Li, L., Li, X., Mi, C.: On the frictional receding contact between a graded layer and an orthotropic substrate indented by a rigid flat-ended stamp. *Mech. Mater.* **158**, 103847 (2021)
38. Erdogan, F.: Mixed boundary value problems in mechanics. In: Nemat-Nasser, S. (Ed.), *Mechanics Today Vol 4*. Oxford: Pergamon Press (1978).
39. Binienda, W.K., Pindera, M.J.: Frictionless contact of layered metal-matrix and polymer-matrix composite half planes. *Compos. Sci. Technol.* **50**(1), 119–128 (1994)